

Analysis of Nanometer-Sized Precipitates Using Advanced TEM[†]

YAMADA Katsumi*¹ SATO Kaoru*² NAKAMICHI Haruo*³

Abstract:

In light of its superior performance in microanalysis, field emission-transmission electron microscopy (FE-TEM) is a useful experimental apparatus to study advanced steels. After a briefly reviewing the recent progress in TEM and its functions for elemental analysis, the authors used FE-TEM for the analysis of a hot-rolled steel with a tensile strength of 780 MPa. According to the results of the authors, the fine precipitates of an MC type (composition: $(Ti_{0.54}Mo_{0.46})C$) was effective in improving the strength of the ferrite matrix. This precipitation strengthening was estimated to be around 250 MPa, based on an analysis of the density of these precipitates. Next, we conducted an EF-TEM experiment on a series of heat-resistant steels that had been strengthened by MX. Fine (V, Cr)N was found to be dispersed in a tempered martensitic steel with superior creep properties. The spatial resolution in elemental mapping of EF-TEM was close to 3 nm in this case.

1. Introduction

The behavior of inclusions and precipitation in steels sometimes directly affects on not only the mechanical properties, but also on microstructural formation and various physical properties. During the production of high-strength low-alloyed steels (HSLA steels), it is important to carefully control the microstructure and precipitation behavior by thermo mechanical processing. For this reason, transmission electron microscopy (TEM) has been used to intensively study the behavior of carbides containing Ti or Nb¹⁾, alloying elements widely used in HSLA steels of the 1980's. The average diameter

of typical precipitates in the late 1970s was about 20 nm. This made it fairly simple to ascertain the size and composition of each precipitate solely using a conventional TEM with instruments attached for elemental analysis. On the other hand, important experimental results have reported the existence of very fine precipitates or atomic clusters with diameters of less than nm. Direct observation using field ion microscopy²⁾ and indirect experimental approaches such as calorimetric measurement³⁾ have provided strong indications of the presence of very fine structures in materials.

Dramatic progress in the analytical capabilities of commercialized TEM, especially field emission TEM (FE-TEM), has recently made it possible to perform elemental analyses with high spatial resolutions of less than several nanometers (and accordingly, with high image resolution). Conventional TEM alone is still difficult to use for the study of very fine precipitation behavior in steels. Recently, however, an advanced TEM with various analytical apparatus attached has made it easier to conduct these types of studies. In this paper the author briefly explain a distinct feature of the advanced TEM used for microstructural analysis in steel research and then describe typical applications for precipitation analysis using this technique.

2. A Distinct Feature of Advanced TEM

2.1 High-Brightness Electron Source

The most remarkable and enabling technical development for the analysis of precipitates within diameters of several nanometers is TEM with the field emission

[†] Originally published in *JFE GIHO* No. 13 (Aug. 2006), p. 18–24



*¹ Dr.Eng.,
Senior Researcher Staff Manager,
Analysis & Characterization Res. Dept.,
Steel Res. Lab.,
JFE Steel



*² Ph.D.,
General Manager, Analysis &
Characterization Res. Dept.,
Steel Res. Lab.,
JFE Steel



*³ Dr.Eng.,
Senior Researcher Deputy Manager,
Analysis & Characterization Res. Dept.,
Steel Res. Lab.,
JFE Steel

Table 1 Comparison of specific values among different types of electron source (Energy width are general values at acceleration voltage 200 kV.)

	Thermo ionic emission (LaB ₆)	Cold Fe W: (100)	Schottky FE W: (310) with ZrO ₂
Brightness (A·cm ⁻² ·sr ⁻¹)	1 to 5 × 10 ⁵	1 × 10 ⁷ to 10 ⁹	5 × 10 ⁸ to 10 ⁹
Energy width (eV)	2	< 0.4	< 0.8
Minimum probe diameter (nm)	10 to 20	< 1.0	1.0
Life time (h)	150 to 200	Permanent	> 9 000
Required vacuum (Torr)	10 ⁻⁵ to 10 ⁻⁶	< 10 ⁻¹⁰	10 ⁻⁸ to 10 ⁻⁹

electron gun (FEG). This method was applied practically from the latter half of 1980's to the first half of 1990's. A scanning transmission electron microscope (STEM) with a cold-type FEG was already available for special-purpose analysis at that time, but difficulties in operation prevented its popularization.

A convenient, easily operable FE-TEM with superior stability and various peripheral equipments has been used commercially for both structural and elemental analyses of local areas in materials, in combination with a nanometer electron probe with high brightness.

Table 1 compares the characteristic values in electron emission sources among Cold-FEG, Schottky FEG and conventional thermal electron emitter (single crystal of LaB₆)^{4,5}. The source of the FEG is considerably brighter than that of LaB₆ (Table 1), which gives it a strong advantage in the use of the small electron probe. Moreover, the electron wave emitted from the FEG is based on a unique principle of electron emission which makes it intrinsically coherent and iso-chromatic. This improves both image resolution and energy resolution when the FEG is applied in combination with the advanced analytical TEM.

2.2 High-Resolution Electron Energy Loss Spectroscopy

Electron energy loss spectroscopy (EELS) is a technology for the analysis of light elements. EELS is especially useful for analyzing the chemical states of particular elements with high energy resolutions of under several electron volt (eV). The technology has been widely used since the commercialization of parallel detection systems in the latter half of 1980's⁶. The performance of EELS analysis has progressed dramatically. The spatial and energy resolution of EELS have been improved by combination with a newly developed FE-TEM with an initial electron energy spread of under 1 eV (Table 1). Thus, the technique is mainly applied to chemical state analyses at well-defined interfaces within nm areas for semiconductor materials. Energy filtering

TEM (EF-TEM), a technology developed in the latter half of 1990's based on this EELS technique, is achievable by attaching post-column energy filtering systems to the existing TEMs⁷.

2.3 Advanced Energy Dispersive X-ray Spectral Mapping

Energy dispersive X-ray spectroscopy (EDXS) with TEM has used mostly in the field of materials science since 1980's. The spatial resolution and signal-to-noise ratio of this analytical method has also been improved in the spectra using a FE-TEM. Multipoint, a line and mapping analysis under STEM mode also become practical with the availability of better statistics on each spectrum and fast data-processing capabilities of recent computer systems. EDXS mapping used to be a method of relative X-ray intensity mapping. Now, however, quantitative data-processing is available by saving whole spectra in the mapping field by the so-called "spectral mapping function."⁸

3. Analysis of Fine (Ti, Mo)C in High-Tensile-Strength Steel with 780 MPa⁹

3.1 Nanometer-Sized Precipitation Hardening Steel

High-tensile-strength steel (TS>350 MPa, TS: Tensile strength), is now used in manufacturing processes in many industries such as automobiles, construction, and shipbuilding. High-tensile-strength steel is particularly useful for reducing the weights of automotive parts while simultaneously improving collision safety. The thin-walled components produced with such steels are very effective in reducing the total emission of carbon dioxides by improving gasoline mileage.

Thus, researchers are fervently studying ways to design and develop steel materials with optimized formability and strength, properties which rarely coexist.

The methods for strengthening steels using solution elements, dislocation, grain refinement and dispersion of fine particles are well known. Combinations of these various methods are thus used in commercially produced steels^{10,11}. Steel usually passes through an austenite phase with a face-centered cubic structure at high temperature before passing through the hot deformation process and changing to a ferrite phase with body-centered cubic structure during or after hot-rolling. The characteristic temperature of the phase transformation can be determined by alloying elements with representative carbon contents. And the cooling condition is also important to control various transformed microstructures such as pearlite, bainite, martensite, and mixtures of them. Highly controlled steels with appropriate microstructures and precipitation are stably produced by a

thermo mechanical controlled process (TMCP) based on the above scientific knowledge¹²⁾.

When the heat is high enough, some alloying elements in a solid solution state in steel making process form precipitate, nitrides, carbides, sulfides, carbosulfides, and inter-metallic compounds in the lower temperature region. The strong carbide former in interstitial free steels scavenges light elements such as carbon and nitrogen thereby changing the matrix to almost pure iron. A dispersion of fine precipitates in the matrix is achieved by adding suitable alloying elements for high-strength steels.

This section describes the results of TEM analysis on fine complex carbonitrides of less than 10 nm in diameter within the steel. This steel was developed using mainly dispersion strengthening techniques. It has a tensile strength of over 780 MPa (80 kgf/mm²).

3.2 Sample and Experimental

The authors studied a newly designed Ti and Mo bearing hot-rolled steel with a basic composition of 0.04C-1.5Mn(mass%). This steel has been developed by optimization of TMCP in which timing of cooling after hot-rolling and a specific coiling temperature relevant to the sufficient precipitation are controlled accurately, in addition to hot-rolling and cooling condition before coiling procedure. The perfect controllability of this TMCP makes it possible to produce materials with an excellent balance between strength (over 780 MPa) and ductility or formability^{13,14)}. This advanced high-tensile strength steel is now used for the underbody components of automobile¹⁵⁾.

The steel used in the analysis of precipitates was coiled at 923 K after hot-rolling procedure. Both specimens for SEM and TEM observation were prepared by electro-chemical polishing using a twinjet-polishing method. The Electrolytic solution was mixture of perchloric acid, methanol, and 2-n-butoxyethanol (blend ratio of 1:10:6). The foil specimens were polished at 25 V and 243 K for FE-SEM and FE-TEM experiments. An elemental analysis was conducted on each fine precipitate using an EDXS attached to the FE-TEM.

3.3 Results

3.3.1 SEM observation

Photo 1 shows a backscattered electron image of Ti and Mo bearing steel with tensile strength of 807 MPa using FE-SEM at an acceleration voltage of 5 kV. Crystallographic channeling contrast is clearly visible. The grain size of the matrix is somewhat coarse, at over 5 μm in diameter and no strong microstructures such as martensite or pearlite can be seen. Based solely on the evidence from Photo 1, we estimate that this steel

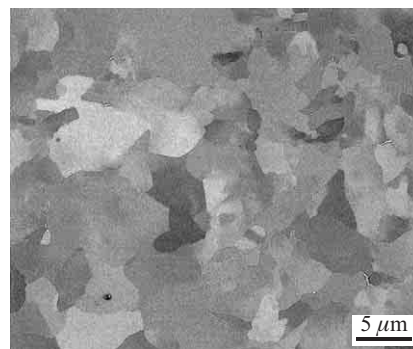


Photo 1 A backscattered electron image of the Ti and Mo bearing steel with tensile strength over 800 MPa

has a tensile strength of up to 500 MPa.

3.3.2 Characterization of precipitates using TEM and elemental analysis

The TEM micrographs shown in **Photos 2(a)** and **(b)** clearly show why this steel has a high strength of over 800 MPa.

An abundance of particles in an average diameter range from about 3 nm to less than 10 nm are observed in the matrix of the steel, as shown in these bright field and dark field images. Large particles with diameters up to 20 nm are also present, but only scarcely. In contrast, the dominant diameter of carbide was reported to be 30 nm in another Ti and Nb bearing high-tensile strength steel with the same tensile strength (780 MPa) and a basic composition of 0.12%C-1.8%Mn¹⁶⁾. The dispersion of finer particles is specific in the steel used in experiment of the authors. Most fine particles are thought to be precipitated in steel when an isothermal transformation from γ to α occurs at the coiling temperature, i.e., at around 923 K. The specific precipitation feature in this case frequently appears as a series of regular, equally

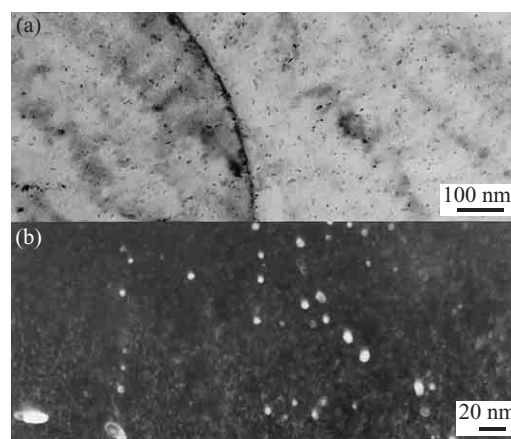


Photo 2 TEM images obtained from the steel of Photo 1 under slightly defocused condition ((a) A bright field image and (b) A dark field image with specific diffraction spot from precipitate)

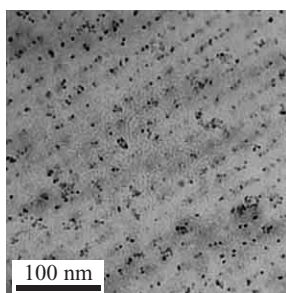


Photo 3 A typical defocused TEM bright field image of the Ti and Mo bearing steel representing periodic line feature which is resulted from interface precipitation during $\gamma \rightarrow \alpha$ transformation at coiling temperature

spaced rows as shown in a **Photo 3**. This arrangement presumably indicates that the precipitation occurs at the interface when γ phase transforms to α phase. Honeycombe have already reported this phenomenon, what they referred to as “interphase precipitation,” in relation to VC in high V steel¹⁷⁾.

Figures 1(a) and **(b)** show EDX spectra obtained from a fine precipitate and matrix in this steel. It is clearly found that Ti, Mo, and C concentrate in the precipitate rather than in the matrix, and this precipitate appears to consist of carbides containing both Ti and Mo. The average atomic ratio between Ti and Mo is estimated to be 0.54:0.46 by a quantitative analysis using Ti and Mo- K_{α} lines.

Mo generally never forms MoC, given that Mo₂C is the more stable carbide in steels at lower temperature. The carbides containing Ti and Mo observed in this experiment were thought to be complex carbides composed of TiC and Mo₂C. With the exception of MC (NaCl

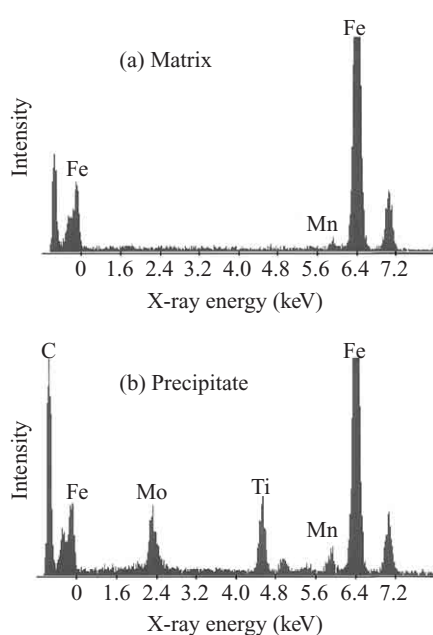


Fig. 1 EDX spectra obtained from (a) matrix and (b) fine precipitate which are embedded in a thin foil specimen

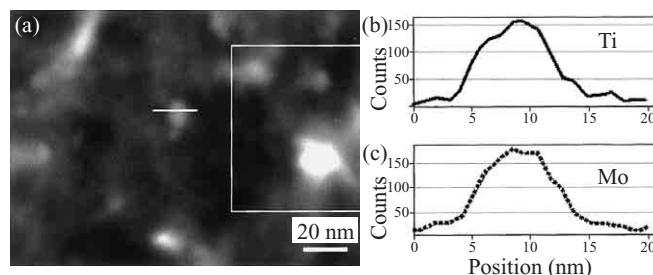


Fig. 2 (a) An annular dark field STEM image of fine (Ti, Mo)C (Line profiles of X-ray intensity of Ti- K_{α} (b) and Mo- L_{α} (c) along with a white line inside (a))

type structure), however, the other carbides were not consistent with the direct nanoprobe electron diffraction pattern from the precipitate and an X-ray diffraction measurement for extracted residues.

Figure 2(a) is an annular dark field image of the (Ti, Mo)C in this steel and Fig. 2(b) is an EDXS line profile with a 1 nm pitch across it. Both were obtained under the STEM mode and using a 1 nm electron probe. The EDXS line analysis is conducted over a distance of about 20 nm crossing a fine precipitate along the line shown inside Fig. 2(a). The rectangular area shown on the right-hand side of Fig. 2(a) is used to compensate for the specimen drift during the collection of the spectra in this EDXS line analysis. As the intensities of the characteristic X-rays of Ti- K_{α} and Mo- L_{α} switch with each other, the ratio of Ti to Mo seems to be constant within the precipitate. Finally, the authors conclude that the fine precipitate in this steel is an MC type carbide in which M contains both Ti and Mo. The typical composition is $(Ti_{0.54}Mo_{0.46})C$.

3.3.3 Estimation of precipitation-hardening

To estimate the precipitation-hardening, the authors use TEM micrographs to calculate the density of the precipitates identified in the previous section. If the authors can obtain a specimen from the extraction replica, the authors can easily measure the precipitates using simple mass absorption contrast. The preparing of the replica specimen is not reliable because the precipitates are too small (about 3 nm in diameter). As an alternative the author use a thin foil specimen.

The method to measure the density of the second phase particles has already been established. In general, we need to consider two points in order to accurately account for the thickness of the observed area: first, the size of the surface precipitate reflects a random cross section; second, there is counting loss of particles along the projected direction of the specimen¹⁷⁾.

Both the surface and overlapping effects are neglected, however, as the particle diameter is less than 10 nm and the thickness of the observed area is less than 50 nm. Another point to note on measuring the density of the second phase in the thin foil specimen is the impor-

tant influence of the diffraction conditions on the contrasts of the small particles. EF-TEM is capable of distinguishing the concentrated areas of specific elements such as Ti or Mo in steels without particle counting loss. Regrettably, however, the method still has limited accuracy and flaws related to the selectivity of the elements. Thus, the author use a simple defocused TEM method for measuring the particle density in this analysis. The application of EF-TEM is to be described in the next chapter.

The second phase particles can be easily detected by a defocused TEM method. In this technique, a clear Fresnel fringe appears at the interface between the matrix and the second phase or void of materials due to drastic change in the electron scattering factor¹⁸⁾. Photos 4(a) and (b) show a focused image and a defocused image with an amount of $2\ \mu\text{m}$ under-focused condition from the same area, respectively. Some of the fine precipitates missing in Photo 4(a) can be detected in Photo 4(b) as shown by the arrows. Though some of the counting loss might be reduced, we must consider the degree of counting loss when the diffraction condition changes in order to ensure a more accurate analysis.

In order to calculate the particle density in an observed area, the authors measure the specimen thickness by the EELS method. This general approach is applied to the thickness measurement in which the intensity ratio between elastic scattering and inelastic scattering is calculated from an EELS spectrum in the observed area¹⁹⁾. In the area shown in Photo 2(a), for example, the specimen thickness is estimated to be 30 nm.

Next, by measuring a randomly selected area, the authors estimate that the nanoparticles in this steel have a dispersion density of $1.7 \times 10^{23}\ \text{m}^{-3}$. The amount of precipitation hardening, σ , is estimated using an above value for dispersion density and the calculated mass density of this precipitate. The Average mass density of this precipitate is calculated based on the composition of the precipitate, $(\text{Ti}_{0.54}\text{Mo}_{0.46})\text{C}$, and the well-defined NaCl type structure. Finally, the Ashby-Orowan formula is applied to estimate σ , as follows²⁰⁾.

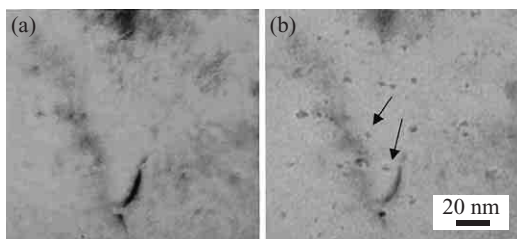


Photo 4 Bright field images of the Ti and Mo bearing steel with tensile strength over 800 MPa ((a) A just focused image and (b) An under focused image of the same area)

$$\sigma(\text{MPa}) = 5.9\sqrt{f} \ln(X/0.00025)/X$$

f : Volume fraction of the precipitates

X : Diameter of the precipitate (μm)

Consequently, σ is estimated to be 250 MPa by applying the value of f and the average diameter X to the above formula.

It remains controversial which model, the Ashby-Orowan mechanism or cutting one²¹⁾, applies more relevantly to the handling of this precipitation hardening. Moreover, the limited TEM observation on which the estimated values are based compromises the accuracy in determining the size and dispersion density of the precipitates. We may require findings on the size distribution as well as the average size in order to more accurately estimate σ . However, the difference in tensile strength between similar steels with and without precipitation hardening is almost 300 MPa. The authors can thus conclude that the estimated value of hardening in this steel is consistent with the difference of these two steels.

4. Analysis of Precipitates in Steels Using EF-TEM

4.1 High-Strength Heat-Resistant Steels Under Controlled MX Precipitation

The so-called heat-resistant steels are used for the components of turbine and boiler tubes in power-generating plants. Excellent fatigue and creep resistance are required for all components used under the high-temperature and high-pressure conditions of these applications. The energy efficiency can be improved and coal consumption can be reduced when the coal-fired electric power plant runs under higher temperature conditions. Researchers in Japan, the U.S., and Europe have been energetically working to meet these requirements by developing advanced ferritic heat-resistant steels.

Various strengthening factors must be accurately controlled in order to improve high-temperature creep resistance as described in section 3.1. As far back as the 1970's and 1980's, Fujita et al. used a metallurgical approach to show the validity of MX type precipitates containing Nb and V in 9–12mass% Cr heat resistant steels^{22,23)}. Their results strongly influenced subsequent studies. The basic design concept of these steels is to use the precipitation of M_{23}C_6 at martensitic lath boundaries and MX within matrix grains to obtain excellent creep resistance for the present ferritic heat-resistant steels. This type of microstructure can be obtained by tempering at over 1023 K after normalization. In our study, the EF-TEM observation and analysis are applied to a model heat-resistant steel in order to optimize the precipitation

hardening of MX.

4.2 Experimental

The author studied a model heat-resistant steel with the following basic composition: 0.08C-9Cr-3.3W-3.0Co-0.2V-0.05Nb-0.05N-0.005B (mass%). The steel was tempered at 1 043 K following water quenched by a solution treatment at 1 473 K. Earlier studies have confirmed that this steel has a superior creep resistance at 923 K under 120 MPa loading condition, presumably because of the finer distribution of MX in comparison to that normally observed in the usual process, and that the steel is normally air cooled from solution treatment²⁴.

Transmission electron microscopy specimen preparation was conducted by a twinjet electro-chemical polishing technique. The solution was 10% perhrolic acid methanol and the polishing was conducted at 253 K and 20 V. Field emission TEM observation was conducted using a FE-TEM attached post-column energy filtering system. This EF-TEM observation has drawn keen attention for its effectiveness in visualizing precipitate without counting loss when the visibility of the fine precipitate depends strongly on the diffraction condition. A group of Austria reported many applications of this method in steel research²⁵. In this study, the authors obtains elemental mapping images of alloying elements such as Cr, V, C, and N using a general three-window method²⁶.

4.3 Results

4.3.1 Visualizing various precipitates in a tempered steel

Photos 5(a)–(e) are typical EF-TEM images representing the usual precipitation state in an ordinal tempered martensitic steel. Precipitates around 100 nm in diameter are easily observed in an elastic scattering image that almost corresponds to a conventional TEM image. Photos 5(b) and (e), the C-K edge and Cr-L edge images, indicate that these large precipitates are $M_{23}C_6$ type carbides. Smaller MX type precipitates are located at interfaces of the lath martensitic structure noticed in the N-K edge and V-L edge mapping images of Photos 5(c) and (d). It is difficult to find homogeneous dispersion of fine MX, this state thought be very effective at improving creep resistance within grains.

4.3.2 EF-TEM image of fine MX and its spatial resolution

Although total amount of precipitate of MX increases according to simple increasing elements of MX former such as N, the creep strength seems to be saturated. A coarsening of MX causes this trend in creep properties.

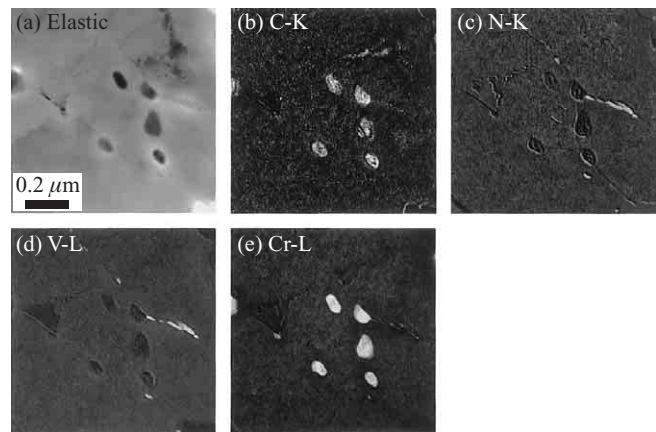


Photo 5 EF-TEM images representing a typical precipitation in a tempered martensitic steel ((a) An elastic scattering, (b) C-K Edge mapping, (c) N-K Edge mapping, (d) V-L Edge mapping, and (e) Cr-L Edge mapping images, respectively)

It can be challenging to avoid or prevent the following: the insoluble large MX after solution treatment, the rapid formation of Nb(C, N) during cooling, and the second precipitation of VN to these Nb(C, N) in the tempering process²⁷. Thus, the authors need to reconsider a conventional heat treatment in order to improve creep resistance by optimizing the MX precipitation.

Photos 6(a), (b), and (c) show EF-TEM images of MX observed in the material crept at 923 K with 120 MPa loading. Fine dispersion of MX in this material was achieved at an initial tempering stage by appropriate MX control. Photo 6 visualizes specific crystallographic relationship between thin platelet MX and martensitic matrix. The elastic image shown in Photo 6(a) provides only an indistinct view of some of the precipitates. The view is clear, however, in Photos 6(b) and (c), the images of the N-K edge and V-L edge.

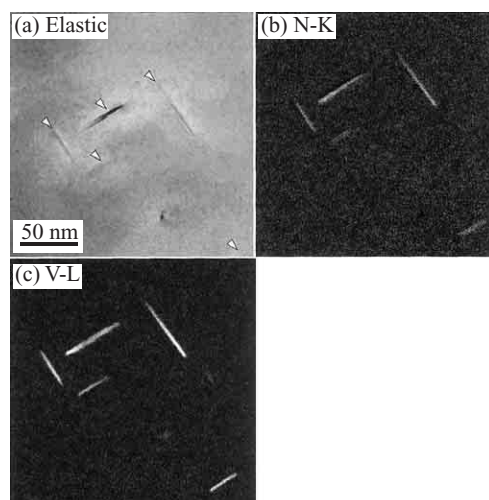


Photo 6 EF-TEM images obtained from a creep ruptured martensitic steel in which fine MX distribution is achieved ((a) An elastic scattering, (b) N-K Edge mapping, and (c) V-K Edge mapping images, respectively)

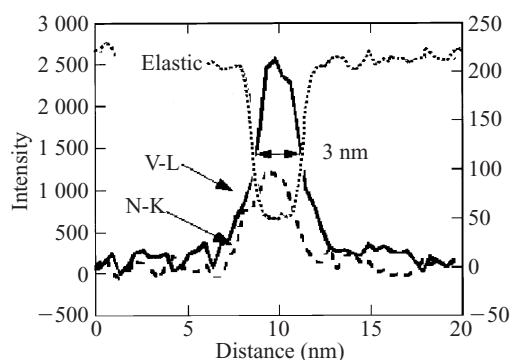


Fig.3 Intensity profiles on the line across a platelet MX shown in Photo 6

Some of the authors have already reported that EF-TEM is very powerful when a platelet precipitate such as this MX aligns in parallel to the direction of specimen thickness²⁸⁾. The results are poorer, however, with the embedded spherical precipitates of around several nanometers in diameter analyzed in section 3.1. **Figure 3** shows line profiles of image intensity across the MX with 20 nanometers distance shown earlier in Photo 6. As we clearly see, the spatial resolution of EF-TEM method is close to 3 nm even in the Nitrogen mapping image.

5. Conclusions

After briefly reviewing a recent method of FE-TEM performed in combination with an advanced TEM technology for elemental analysis, the author analyzed the precipitation in steels and obtained the following results.

- (1) The spatial resolution of single nanometers was practically obtained by elemental analyses such as EDXS and EELS performed in combination with FE-TEM.
- (2) The composition of fine MC type carbide was determined to be $(\text{Ti}_{0.54}\text{Mo}_{0.46})\text{C}$ from an FE-TEM analysis of steel strengthened to over 800 MPa by fine dispersion of the MC type precipitates.
- (3) Precipitation hardening was estimated to be about 250 MPa, based on an analysis of the average size and distribution of the above fine MC in this Ti and Mo bearing steel.
- (4) A spatial resolution of 3 nm could be achieved even in the Nitrogen mapping of MX when EF-TEM was applied to fine platelet MX observed in a heat-resistant steel with fine dispersion of MX.

References

- 1) For example, Ouchi, C.; Sanpei, T.; Okita, T.; Kozasu, I. Microstructural changes of austenite during hot rolling and

- their effects on transformation kinetics. Proc. of the Hot Deformation of Austenite. Balance, J. B. ed. New York, The Metallurgical Society of AIME, 1977, p. 316–340.
- 2) For example, Cerezo, A.; Godfrey, T. J.; Sijbrandij, S. J.; Smith, G. D.; Warren, P. J. Rev. Sci. Instrum. vol. 69, 1998, p. 49.
- 3) For example, Tokunaga, Y.; Morishige, M. Nippon Kinzokugaggaishi. vol. 43, 1979, p. 834–840.
- 4) Reimer, Ludwig. Transmission electron microscopy. Springer Series in Optical Sciences. vol. 36, 1984, p. 86–99.
- 5) Mul, Peter M.; Bormans, Ben J. H.; Otten, Max. Philips Electron Optics Bulltin. no. 130, 1991.
- 6) For example, Colliex, C.; Manoubi, T.; Krivanek, O. L. EELS in the electron microscope: A review of present trends. J. Electron Microsc. vol. 35, no. 4, 1986, p. 307–313.
- 7) For example, Krivanek, O. L.; Gubbens, A. J.; Dellby, N.; Meyer, C. E. Microsc. Microanal. Microstruc. vol. 3, 1992, p. 187–199.
- 8) For example, Watanabe, M.; Williams, D. B. Proc. of 14th Symp. of Analytical Electron microscopy. 1998, p. 33–38.
- 9) Sato, K.; Nakamichi, H.; Yamada, K. Characterization of nanometer-sized complex carbide in steel using electron microscopy. Kenbikyoku. vol. 40, no. 3, 2005, p. 183–187.
- 10) Maki, M. Tokushukou. vol.52, 2003, p. 4–8.
- 11) Maki, M. Kinzoku. vol. 71, 2001, p. 771–780.
- 12) For example, Ouchi, C.; Okita, T.; Yamamoto, S. Trans. ISIJ. vol. 22, 1982, p. 608.
- 13) Funakawa, Y.; Shiozaki, T.; Tomita, K.; Yamamoto, T.; Maeda, E. Development of high strength hot-rolled sheet steel consisting of ferrite and nanometer-sized carbides. ISIJ Int. vol. 44, no. 11, 2004, p. 1945–1951.
- 14) Funakawa, Y.; Tomita, K. Tokushukou. vol. 52, 2003, p. 37–38.
- 15) Seto, K. Kougyozairyo. vol. 52, 2004, p. 22–25.
- 16) Honeycomb, R. W. K. Metall. Trans. A. vol. 7A, 1976, p. 915–936.
- 17) Hirsch, P. B.; Howie, A.; Nocolson, R. B.; Pashley, D. W.; Whelan, M. J. Electron Microscopy of Thin Crystals. London, Butterworth, 1965, p. 424–427.
- 18) Iijima, S. Optik. vol. 47, 1977, p. 437–452.
- 19) Egerton, R. F. Electron Energy Loss Spectroscopy in the Electron Microscope. 2nd ed. Plenum Press, New York, 1986, p. 304–305.
- 20) William, C. The Physical Metallurgy of Steels. Koda, S. et al, transl. Maruzen, 1985, p.213. (Japanese)
- 21) Strudel, J. L. Physical Metallurgy 2nd ed. By Cahn, R. W.; Haasen, P. North-Holland Physics Publishing, Amsterdam, 1983, p. 1421–1486.
- 22) Fujita, T.; Asakura, K.; Sawada, T.; Takamatsu, T.; Otaguro, Y. Creep rupture strength and microstructure of low C-10Cr-2Mo heat-resisting steels with V and Nb. Metall. Trans. vol. 12A, 1981, p. 1071.
- 23) Asakura, K.; Fujita, T. Report of the 123rd committee on Heat-Resisting Metals and Alloys. vol. 27, 1986, no. 3, p. 13.
- 24) Yamada, K.; Igarashi, M.; Muneki, S.; Abe, F. Effect of heat treatment on precipitation kinetics in high-Cr ferritic steels. ISIJ Int. vol. 42, 2002, no. 7, p. 779–784.
- 25) For example, available from <http://www.felmi-zfe.tugraz.> (accessed 2006-01).
- 26) Egerton, R. F. Electron Energy Loss Spectroscopy in the Electron Microscope. 2nd ed. Plenum Press, New York, 1986, p. 330–334.
- 27) Yamada, K.; Igarashi, M.; Muneki, S.; Abe, F. Creep properties affected by morphology of MX in high-Cr ferritic steels. ISIJ Int. vol. 41, Suppl., 2001, S116–120.
- 28) Yamada, K.; Sato, K.; Kurata, H.; Kobayashi, T. Visualization of carbon in steels using energy filtering TEM. J. of Electron Microscopy. vol. 48, 1999, no1, p. 9–15.